Thermally Cross-Linked PNVP Films As Antifouling Coatings for Biomedical Applications

Andrew M. Telford,[†,‡] Michael James,[§,∥] Laurence Meagher,[⊥] and Chiara Neto*[,†]

School of Chemistry, Building F11, The University of Sydney, New South Wales 2006, Australia, Bragg Institute, Australian Nuclear Science and Technology Organisation (ANSTO), PMB 1, Menai, New South Wales 2234, Australia, School of Chemistry, The University of New South Wales, New South Wales 2052, Australia, CSIRO Molecular and Health Technologies, Bag 10, Clayton South, Victoria 3169, Australia, and CSIRO Future Manufacturing National Research Flagship, Clayton, Victoria 3168, Australia

ABSTRACT Protein repellent coatings are widely applied to biomedical devices in order to reduce the nonspecific adhesion of plasma proteins, which can lead to failure of the device. Poly(*N*-vinylpyrrolidone) (PNVP) is a neutral, hydrophilic polymer with outstanding antifouling properties often used in these applications. In this paper, we characterize for the first time a cross-linking mechanism that spontaneously occurs in PNVP films upon thermal annealing. The degree of cross-linking of PNVP films and their solubility in water can be tailored by controlling the annealing, with no need for additional chemical treatment or irradiation. The physicochemical properties of the cross-linked films were investigated by X-ray photoelectron spectroscopy, infrared spectroscopy, neutron and X-ray reflectometry, ellipsometry, and atomic force microscopy, and a mechanism for the thermally induced cross-linking based on radical formation was proposed. The treated films are insoluble in water and robust upon immersion in harsh acid environment, and maintain the excellent protein-repellent properties of unmodified PNVP, as demonstrated by testing fibrinogen and immunoglobulin G adsorption with a quartz crystal microbalance. Thermal cross-linking of PNVP films could be exploited in a wide range of biotechnological applications to give antifouling properties to objects of any size, essentially making this an alternative to high-tech surface modification techniques.

KEYWORDS: biocompatibility • antifouling • protein adsorption • cross-linking • PNVP

INTRODUCTION

Surgical implantation procedures such as hip replacement (1), artificial cochlea implantation (2), and stent implantation (3), have become more and more widespread in medicine and are now routinely performed. In vivo biosensing to continuously monitor the concentration of analytes in the bloodstream, such as glucose in diabetic patients, is also common (4−6). The performance of biomaterials and biosensing devices however can be hampered by biofouling, i.e., the nonspecific adsorption of proteins and biomolecules from solution (7). When an extraneous object comes in contact with a tissue, it is rapidly coated by proteins in the first instance, and then platelets and immune cells. In some cases, a fibrous capsule can develop that can severely limit functioning of the device. Nonspecific protein adsorption on the surfaces of biomedical devices can also allow attachment of bacteria, and the formation of a biofilm which can be very difficult to treat with antibiotics (8). In addition, once injected in the bloodstream, drug delivery particles or magnetic particles for medical imaging are quickly covered with plasma proteins before they can perform their function (9, 10). In vivo devices such as biomedical implants inserted in the human body may provoke a dramatic cascade of events that eventually causes surface-induced thrombosis (11). The accumulation of proteins on the surface of contact lenses can also lead to infections (12). An effective strategy to overcome the nonspecific adsorption of proteins is to coat the surface with an antifouling coating that makes it inert to processes in the living body, and therefore more biocompatible.

Hydrophilic polymers, such as poly(ethylene glycols) (13−15), poly(*N*-vinylpyrrolidone) (16), and polymers containing zwitterionic functionalities (17), are widely used as antifouling coatings for medical devices, because their properties can be finely tailored and surfaces can easily be coated with them (18−20).

Poly(*N*-vinylpyrrolidone) (PNVP, top of Figure 8) is well-known for its antifouling properties, widely used and readily available (21−24). PNVP is nontoxic, water-soluble, and completely biocompatible in humans (25, 26). It is used as a binder in many pharmaceutical tablets (27), in dental care and wound care products (28, 29), in cosmetics (30), in contact lenses (31), and as a plasma expander (32). In its bulk cross-linked form (as a hydrogel) it is used in drug delivery systems (33, 34). However, because of its solubility

* Corresponding author. E-mail chiara.neto@sydney.edu.au. Fax: +61-2-93513329.
Received for review May 10, 2010 and accepted July 7, 2010
† The University of Sydney.
‡ CSIRO Future Manufacturing National Research Flagship.
§ Australian Nuclear Science and Technology Organisation.
∥ The University of New South Wales.
⊥ CSIRO Molecular and Health Technologies.
DOI: 10.1021/am100406j

in water, PNVP coatings are only useful for contact with body fluids after treatment or modification to make the polymer insoluble.

PNVP coatings are often prepared by grafting the molecules from a supporting substrate, using surface initiated polymerization (16). In a good solvent regime and at high surface coverage, the grafted hydrophilic chains form a "brush" that stretches out of the surface and into the solvent, and reduces protein adsorption due mainly to steric repulsion (35, 36). The grafting technique, although effective, requires a number of chemical synthetic steps.

PNVP coatings are also commonly cross-linked in a hydrogel, using as cross-linking agents either an electron beam (37), redox reactions (38), or UV-activated molecules (39). In the case of radiation-induced cross-linking it is believed that the water in the hydrogel is necessary to allow chain mobility and produce an effective cross-linking (40, 41), so plain (100%) PNVP thin films have rarely been investigated (42). The generation of radicals in PNVP by thermal annealing has been previously proposed (43), but thermally induced cross-linking has never been characterized in thin films, nor have such films been employed in biomedical applications.

In this work, we demonstrate for the first time a method to prepare cross-linked PNVP antifouling coatings on surfaces of any geometry and size by simple and cost-effective techniques such as spin- or dip-coating and thermal annealing, without the use of cross-linking agents or high energy radiation. Under specific annealing conditions, PNVP films spontaneously cross-link, becoming insoluble in water and many other solvents, while still maintaining the antifouling properties of unmodified PNVP. The degree and the speed of the process can be tuned by controlling the temperature.

MATERIALS AND METHODS

Materials. Silicon wafers coated with a native oxide layer (MMRC Pty Ltd., Malvern VIC Australia) were cut into squares and used as substrates. To clean them, the silicon substrates were sonicated in distilled ethanol and in distilled acetone. After blow drying with pure nitrogen, they were cleaned with a CO_2 snow jet to remove dust, and treated further using a plasma cleaner (Harrick Plasma, Itacha NY, model PDC-002) to remove organic contaminants.

Poly (*N*-vinylpyrrolidone) 29 000 g/mol (95%, Sigma-Aldrich) was used as-received. Ethanol (99%) and acetone (99%, Sigma-Aldrich) were distilled before use. Thermal gravimetric analysis (TGA) and differential scanning calorimetry (DSC) on the polymer powder were obtained using TA Instruments TGA 2950 and DSC 2920, respectively. Human serum fibrinogen (FGN) and bovine serum immunoglobulin G (IgG) were purchased from Sigma-Aldrich.

A phosphate buffer saline solution (PBS) was prepared by mixing $NaH_2PO_4 \cdot 7H_2O$ (10 mM), KCl (3 mM) and NaCl (140 mM) in MILLI-Q water and adjusting the pH to 7.4 using 1 M NaOH solution. The buffer solution was filtered using (0.45 μm) cellulose filters.

Surface Preparation. PNVP films were prepared by spin coating (Laurell Technologies Co., PA, model WS400B-6NPP-LITE) a 10 mg/mL filtered ethanol solution of PNVP (3000 rpm for 1 min). Polystyrene (PS) films were prepared in a similar way from a 10 mg/mL toluene solution (4000 rpm for 1 min). The average thickness of the PNVP films obtained was 40 $\pm$ 1 nm, determined by spectroscopic ellipsometry (J.A. Woollam Co. Inc., model M-2000 V). The wetting properties of the PNVP films were investigated by measuring the static contact angle of 5−10 μL sessile droplets of MILLI-Q water with a KSV CAM200 Contact Angle System (KSV Instruments Ltd., Helsinki, Finland).

Annealing of PNVP films was performed on a hot plate with fine temperature control (ATV Technologie GmbH Muenchen, model TR-124) in air. Noncross-linked PNVP was eliminated by rinsing the films under 150 mL of MILLI-Q water. After rinsing, the films were blown dry with pure nitrogen and dried on a hot plate at 100 °C for 30 min to remove residual water.

Film Characterization. The films were characterized using X-ray and neutron reflectometry at the Australian Nuclear Science and Technology Organization (ANSTO) in Sydney. Four films were characterized after different annealing and washing procedures. X-ray reflectivity profiles were measured on a Panalytical Ltd. X'Pert Pro Reflectometer using Cu Kα X-ray radiation (λ = 1.54056 Å). The X-ray beam was focused using a Göbel mirror and collimated with 0.2 mm pre- and postsample slits. Reflectivity data were collected over the angular range $0.05° \leq \theta \leq 5.00°$, with a step size of 0.010° and counting times of 10 s per step.

Neutron reflectivity data were measured on these polymer films using the Platypus time-of-flight neutron reflectometer (44) and a cold neutron spectrum (3.0 Å $\leq \lambda \leq$ 18.0 Å) at the OPAL 20 MW research reactor. Twenty-three Hz neutron pulses were generated using a disk chopper system (EADS Astrium GmbH) in the medium resolution mode ($\Delta\lambda/\lambda$ = 4%), and recorded on a 2-dimensional helium-3 neutron detector (Denex GmbH). Reflected beam spectra were collected for each of the as-prepared and modified PNVP films at 0.5° for 2 h (0.5 mm slits) and 2.0° for 6 h (2 mm slits) respectively. Neutron reflectivity data were also collected for one film at 4.0° for 8 h (4.0 mm slits). Direct beam measurements were collected under the same collimation conditions for 1 h each.

Structural parameters for these PNVP films were refined using the MOTOFIT (45) reflectivity analysis software with reflectivity data as a function of the momentum transfer vector Q (= $4\pi(\sin\theta)/\lambda$). In the fitting routines, the Levenberg−Marquardt method was selected to minimize χ^2 values by varying the film thickness, roughness and scattering length density (SLD). One or two layers models were used, and single-layer models were chosen when no significant improvement in the fitting quality was observed upon the introduction of an additional layer. Because of the lack of scattering contrast between silicon (SLD = 2.01×10^{-5} Å^{-2}) and the native silicon oxide layer (SLD = 1.89×10^{-5} Å^{-2}), the silicon oxide layer was omitted from structure refinements using X-ray reflectivity data. In the case of models refined using neutron reflectivity data, an additional ~10 Å layer was included adjacent to the silicon (SLD = 2.07×10^{-6} Å^{-2}), representing the native oxide layer (SLD = 3.47×10^{-6} Å^{-2}).

Investigations of the chemical composition of untreated and annealed films were carried out by transmission Fourier transform infrared spectroscopy (FTIR) using a Bruker Vertex 80v FTIR spectrophotometer with a Hyperion 3000 FPA microscope system. The data were analyzed using the OPUS software provided by the manufacturer. Each spectrum was corrected for CO_2 and H_2O absorption.

Further information about the elemental makeup of these as-prepared and annealed (and not rinsed) PNVP thin films was obtained from X-ray photoelectron spectroscopy (XPS) data, collected using an Escalab 220i-XL spectrometer (VG, UK) with monochromated Al Kα exciting radiation (energy 1486.6 eV). Typical operating conditions were power 120 W (10 kV, 12 mA), spot size 1 mm^2. Wide range spectra were collected with a step width of 1 eV and high-resolution spectra with a step width of 0.1 eV.

Because of the fact that cross-linked PNVP is insoluble, we could relate the percentage of cross-linked film to the residual film thickness after rinsing with MILLI-Q water. The cross-linking dependence on annealing time and temperature was investigated using spectroscopic ellipsometry. The films were annealed at different temperatures and for different times (160, 170, 180, and 200 °C for 30 min, 1 h, and 3 h) and the thickness of the films was measured. The films were then rinsed with MILLI-Q water, dried as described above, and the thickness remeasured. Two samples were analyzed for each annealing time and temperature. Ellipsometry was also used to investigate the stability of annealed PNVP films after soaking in water for extended periods (200 °C, 3 h). Film thickness was measured after annealing and again after soaking in water for specified periods of time and drying.

Topography and surface roughness of the PNVP films were investigated using an Asylum Research (San Francisco CA) MFP-3D-SA atomic force microscope (AFM) in tapping mode.

Protein Adsorption. A quartz crystal microbalance (QCM-D, Qsense model E4) was used to investigate the adsorption of two proteins, fibrinogen (FGN) and immunoglobulin G (IgG), on PNVP films, PS films, and gold. The quartz crystal sensors used were gold coated, with a primary resonant frequency of 5 MHz. The PS and the PNVP films were prepared by spin coating onto these sensors as described above. The PNVP film was annealed at 200 °C for 3 h to obtain complete cross-linking.

Before each measurement, the QCM crystals were all initially equilibrated in PBS. Protein adsorption experiments were then carried out in parallel using a 1 mg/mL FGN solution in PBS on one set of crystals, and a 1 mg/mL IgG solution in PBS on another set. The protein solutions were passed over the sensor at a flow rate of 100 μL/minute for 20 min, the flow stopped, and the surfaces left in contact with the protein solution for about 1 h. Finally, the surfaces were rinsed with PBS. The whole analysis was performed under temperature control at 37 °C. The adsorbed protein was quantified using the Sauerbrey equation:

$$\Delta m = \Delta f \sqrt{(p_q \mu_q)}/2f_0$$

where Δm is the adsorbed mass (g cm^{-2}), Δf is the frequency shift (Hz, measured immediately before the rinsing with PBS), p_q is the density of quartz (2.648 g cm^{-3}), μ_q is the shear modulus of quartz for AT-cut crystal (2.947×10^{11} g cm^{-1} s^{-2}), and f_0 is the fundamental resonant frequency of the crystal.

RESULTS

Thermal Gravimetric Analysis. The PNVP powder used to prepare all our samples was characterized by thermal gravimetric analysis (TGA) to determine the mass loss at the annealing conditions used in the preparation of our coatings, as well as to ensure that no significant decomposition of the polymer was taking place. The powder was quickly heated (in less than 2 min) to 200 °C and left at this temperature for 3 h either in air or in nitrogen. The TGA profiles in Figure 1 show a small decrease in mass (about 8−9%) in the first minutes of the annealing both in air and in nitrogen. This initial mass loss was due to a small quantity of water retained by PNVP (up to 5% according to the manufacturer product description, given that PNVP is a hydrophilic polymer), as well as impurities such as unreacted monomer. After the first few minutes in a nitrogen atmosphere, the mass of the PNVP sample remained constant for the rest of the measurement time (3 h), while in air the sample mass increased by about 0.1%, which could be interpreted as a sign of a mild oxidation. Otherwise, the polymer did not decompose nor gain substantial mass after 3 h of thermal annealing at 200 °C both in air and in nitrogen.

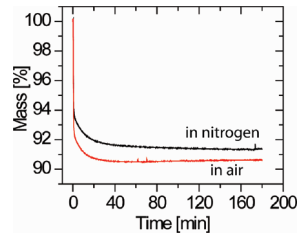

FIGURE 1. TGA profile of PNVP. The polymer in its powder form was heated to 200 °C for 3 h in air and in nitrogen.

Previous studies have revealed that thermal treatment of PNVP in an oxygen atmosphere gave rise to volatile degraded products at lower temperatures than in an inert atmosphere (46), with degradation of the polymer occurring above 250 °C; a temperature considerably higher than the 200 °C used in our study. At these elevated temperatures, as high as 400 °C, the presence of an oxygen atmosphere has been shown to lead to the formation of peroxide residues, which decompose and give rise to the formation of active radicals (46). The mechanism of photooxidation of PNVP films under UV light has also been investigated before and leads primarily to the formation of insoluble fractions (42). DSC results identify the glass transition temperature (T_g) of PNVP to be at approximately 160 °C (see the Supporting Information, Figure S1).

Atomic Force Microscopy. Tapping mode atomic force microscopy (AFM) characterization of the PNVP films showed that the morphology of the films remained featureless, and did not change significantly upon thermal annealing (see the Supporting Information, Figure S2). Root mean square (rms) roughness values, before (203 ± 1 pm) and after (252 ± 8 pm) annealing indicated that these thin films were very smooth and similar to that of the underlying Si substrate (typically below 200 pm).

X-ray Photoelectron Spectroscopy. XPS data were collected on an untreated film and on a film annealed at 200 °C for 3 h, prior to rinsing with water. Figure 2 shows the wide range XPS spectra of the untreated and treated films (a) as well as high resolution C 1s (b), N 1s (c), and O 1s (d) spectra. In the figure, the data for the untreated film was shifted up by 20 000 counts/s in part a and by 2000 in parts b−d to highlight differences before and after the treatment. The C 1s spectrum (Figure 2b) was fitted with 5 different components: component A is due to the presence of aliphatic hydrocarbon (C−C, C−H), component B is due to secondary shifted aliphatic carbon, component C is due to the presence of C−N/C−O groups, component D is due to the presence of C═O/O−C−O/N−C═O groups, and component E is most likely due to the presence of carboxylic acids. The presence of component E in the untreated film indicated that the polymer as-received was already slightly oxidized. This peak was more intense in the annealed sample data, suggesting that the polymer underwent some degree of oxidation as a

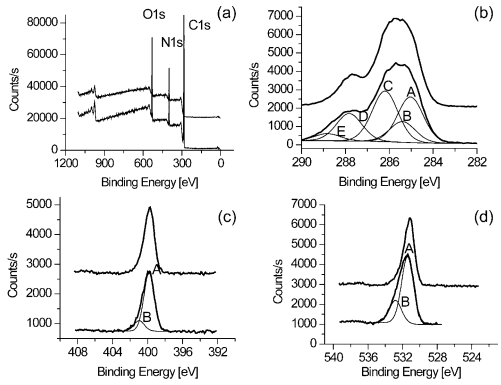

FIGURE 2. XPS data collected on an untreated PNVP film (upper curves), and on a film annealed at 200 °C for 3 h (lower curves, including fits). (a) Wide scan spectrum and high-resolution spectra for (b) C 1s, (c) N 1s, and (d) O 1s.

Table 1. XPS Elemental Composition Data for Untreated PNVP Film and a Thermally Modified Film Following Annealing at 200 °C for 3 h

label	peak binding energy (eV)	normalized area (%)	total normalized area (%)
	As-Prepared Film		
C1s A	285.0	15.1	C1s = 77.0%
C1s B	285.3	18.7	
C1s C	286.1	28.5	
C1s D	287.8	13.7	
C1s E	289.0	0.9	
N1s A	399.9	10.0	N1s = 11.7%
N1s B	401.0	1.7	
O1s A	531.3	9.7	O1s = 11.3%
O1s B	532.5	1.7	
	After Annealing at 200 °C, 3 h		
C1s A	285.0	21.9	C1s = 72.8%
C1s B	285.4	10.0	
C1s C	286.2	24.3	
C1s D	287.8	13.2	
C1s E	288.8	3.4	
N1s A	399.9	9.6	N1s = 11.4%
N1s B	401.1	1.7	
O1s A	531.5	11.9	O1s = 15.8%
O1s B	532.9	4.0	

result of the thermal treatment. The N 1s spectra obtained before and after annealing did not show any remarkable differences (Figure 2c). Analysis of the O 1s spectrum for the annealed film (Figure 2d) suggested an increase in component B that was due to the presence of O with a higher oxidation state (e.g., C−OH bonds), supporting the possibility of slight oxidation of the polymer.

Table 1 summarizes the carbon, nitrogen, and oxygen content in the two samples. The oxygen content increased by about 30% upon annealing, the C content decreased by 5% and the N content was essentially unchanged. These data were used to obtain the hydrogen content in the two types of film (untreated and annealed), when used in combination with the neutron reflectivity data (see below).

X-ray and Neutron Reflectometry. The degree of cross-linking of PNVP films induced by thermal annealing was characterized by X-ray and neutron reflectometry, by investigating films after increasing annealing times (5 min, film 1; 30 and 60 min, film 2; and 180 min, film 3).

X-ray and neutron reflectivity profiles for a PNVP coating (film 1) in the as-prepared state (trace a), after annealing for 5 min at 200 °C (trace b), and after rinsing with 30 mL Milli-Q water (trace c) are shown in Figures S3 and S4, respectively (see the Supporting Information). Refined structural parameters for these films are given in Table 2. The structure of the untreated film was refined using a single layer model for both the X-ray and neutron reflectivity data, indicating a film of ∼44 nm in thickness and a surface roughness of less than 1 nm. On the basis of the monomer composition C_6H_9NO and the observed SLD values, the mass density of this film was found to be 0.79 g/cm^3.

Following the annealing of film 1 at 200 °C for 5 min, X-ray reflectivity data were fitted by a single-layer model (see the Supporting Information, Figure S3, trace b). Comparison between these data and that for the as-prepared film (trace a) shows more pronounced Kiessig fringes with wider spacing, indicating a slightly thinner (43 nm), denser film after annealing and rinsing. An adequate fit to the neutron reflectivity data was not possible using a single-layer model. A two layer model was subsequently used to fit these data (see the Supporting Information, Figure S4, trace b), indicating a 9.9 nm less dense upper layer (SLD of 0.89 × 10^6 Å^{-2}) and a 33.4 nm more dense lower layer (SLD of 1.02 × 10^6 Å^{-2}) (Table 2). The uppermost surface of the film was found to be relatively smooth (0.8 nm), although the interfacial region between the two layers was found to be quite diffuse (5.8 nm) indicating a gradient in composition.

Rinsing with a small amount of water (30 mL) saw a further reduction in film thickness and a substantial increase in surface roughness, which is evident in the damping of fringes at high Q. Both X-ray (see the Supporting Information, Figure S3, trace c) and neutron (see the Supporting Information, Figure S4, trace c) reflectivity profiles required a two layer model in order to produce an adequate fit. The refined structural data (Table 2) indicates a partial removal of the upper non-cross-linked polymer layer, a diffuse interfacial layer, and a denser base layer adjacent to the Si wafer.

Figure 3A shows observed (points) and calculated (solid black lines) X-ray reflectivity profiles for a PNVP coating (film 2) in the as-prepared state (trace a), after annealing for 30 min at 200 °C (trace b), and after subsequent annealing for 60 min at 200 °C (trace c). Prior to measurement, the annealed surfaces were rinsed with MILLI-Q water and then dried. Analogous neutron reflectivity data after each stage of processing and are shown in Figure 3B. Refined structural parameters for film 2 based on single layer models are given in Table 2.

The PNVP film was found to decrease in thickness from 37.7 nm in the as-prepared state, to 33.3 nm, and 29.9 nm upon subsequent annealing for 30 and 60 min, respectively (a decrease in thickness of about 11% after 30 min, and of about 21% after 60 min). Annealing of this film also led to

Table 2. Refined Structural Parameters from X-ray and Neutron Reflectivity Data for As-Prepared PNVP films, and for Films Annealed at 200 °C for 5, 30, 60, and 180 Min, with Estimated Standard Deviations in Parentheses

	annealing temperature							
	film 1			film 2			film 3	
	as-prepared	200 °C	200 °C	as-prepared	200 °C	200 °C	as-prepared	200 °C
annealing time (min)		5	5		30	60		180
rinsed with water (mL)			30		150			150
				X-rays				
film thickness (nm)	44.1(1)	43.0(1)	U: 1.8(3)[a] L: 4.3(1)	37.7(1)	33.3(1)	29.9(1)	50.6(3)	37.0(2)
SLD ($\times 10^6$ Å^{-2})	7.21(2)	8.45(2)	U: 4.59(2)[a] L:8.43(3)	7.48(2)	7.68(2)	7.54(2)	7.62(2)	10.35(3)
surface roughness (nm)	0.6(1)	0.6(1)	U: 1.4(2)[a] L: 0.8(1)	0.4(1)	0.6(1)	0.6(1)	0.9(1)	0.8(1)
				Neutrons				
film thickness (nm)	44.6(3)	U: 9.9(2)[a] L: 33.4(3)	U: 9.0(2)[a] L: 26.7(3)	38.2(3)	33.6(2)	30.5(2)	50.3(4)	37.5(3)
SLD ($\times 10^6$ Å^{-2})	0.92(3)	U: 0.89(3) L: 1.02(4)	U: 0.68(3)[a] L: 0.90(3)	0.93(3)	1.48(2)	1.65(2)	0.94(1)	1.98(2)
surface roughness (nm)	0.7(2)	U: 0.8(2) L: 5.8(3)	U: 2.3(2)[a] L: 3.6(3)	0.5(1)	0.8(2)	0.8(1)	1.1(1)	0.7(2)

[a] "U" indicates the upper layer of film, and "L" the lower layer.

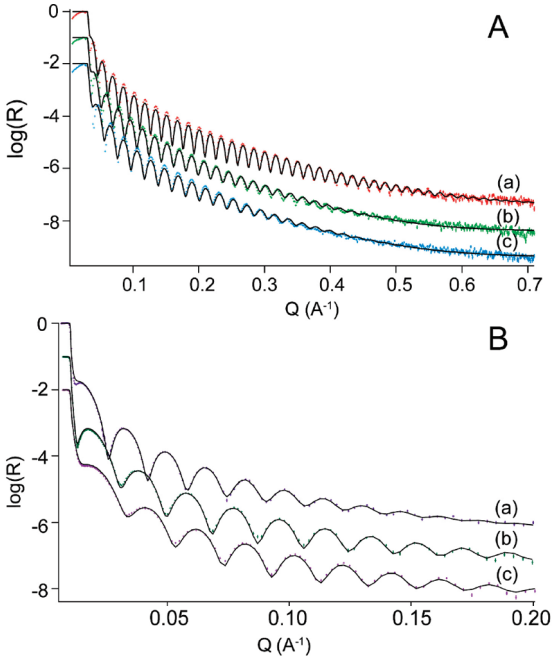

FIGURE 3. (A) Observed (points) and calculated (solid lines) X-ray reflectivity and (B) neutron reflectivity data for (a) an untreated PNVP coating (film 2), (b) after annealing the sample for 30 min at 200 °C, and (c) 60 min at 200 °C. Data have been offset be a factor of 0.1 and 0.001 for traces b and c for clarity.

a small increase in surface roughness (from 0.4 to 0.6 nm) as indicated by the damping of the Kiessig fringes for data sets b and c in Figure 3A. On the basis of these X-ray reflectivity data, relatively little change was observed for the scattering length density upon annealing.

The neutron reflectivity data for this film on the other hand indicate a different picture. Refinement of the as-prepared film (trace a) in Figure 3B gave essentially the same model as for the as-prepared film of Figure S4 in the Supporting Information; a smooth uniform film with a mass density of 0.81 g/cm^3. Refinement of the neutron reflectivity data (trace b and c) from the annealed samples revealed significantly increased SLD values: 1.48 $\times$ 10^6 Å^{-2} (after 30 min) and 1.65 $\times$ 10^6 Å^{-2} (after 60 min). The combination of little variation in X-ray SLD and increases in the neutron SLD suggest that the mass density of the annealed films remained relatively constant, whereas the hydrogen content decreased compared to the as-prepared film.

Panels A and B in Figure 4 show X-ray and neutron reflectivity profiles respectively for the as-prepared coating (film 3) (trace a), and the film after annealing at 200 °C for 3 h and rinsing (trace b) with the refined structural parameters reported in Table 2. These refinements reveal the film thickness decreased from 50.6 nm for the as-prepared film, to 37 nm for the annealed film. This densification is reflected in an increase in scattering length density: from 7.62 to 10.35 $\times$ 10^6 Å^{-2} for X-rays, and from 0.94 to 1.98 $\times$ 10^6 Å^{-2} for neutrons. In the case of the neutron reflectivity data (Figure 4Bb) the Kiessig fringes showed much weaker oscillations for the annealed film compared to the as-prepared film (Figure 4Ba); this is an indication of the poor scattering length density contrast between the annealed film and the silicon substrate.

In summary, analysis of these reflectivity data on films annealed for increasing amounts of time indicated a gradual cross-linking, starting from the bottom of the film (side closer to the heating source), and then extending with time to the rest of the film. Thermal annealing led to a slight increase in mass density of these films, with a consequent increase

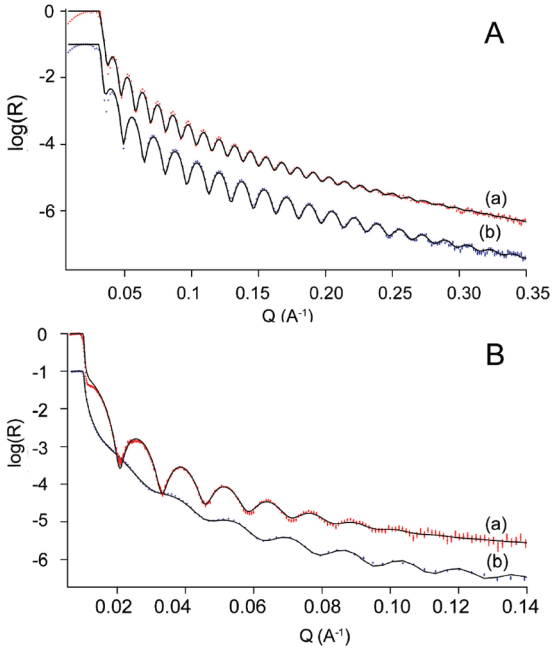

FIGURE 4. (A) X-ray reflectivity and (B) neutron reflectivity data for (a) an untreated PNVP coating (film 3) and (b) after annealing the sample for 180 min at 200 °C and rinsing. Data have been offset be a factor of 0.1 for traces b for clarity.

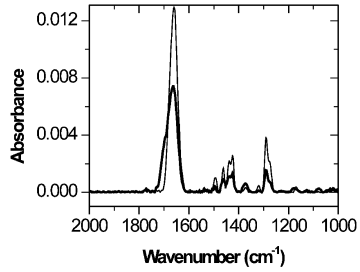

FIGURE 5. Fourier transform infrared (FTIR) spectra of an untreated PNVP film (thin line) and PNVP film annealed at 200 °C for 3 h (thicker line).

in X-ray scattering length density. The scattering length density of the non-cross-linked portion of these films was the same as the untreated polymer, indicating that cross-linking was indeed the main phenomenon occurring, and no other degradation or chemical modification were observed. In addition, the residual non-cross-linked polymer that was present after short annealing times retained a high degree of solubility in water. The combined neutron and X-ray reflectivity data for the annealed samples suggest that at intermediate annealing times (30 and 60 min) the mass density of the annealed films remained relatively constant, whereas the hydrogen content decreased compared to the as-prepared film.

Transmission FTIR. Figure 5 shows transmission FTIR spectra for a 40 nm thick PNVP untreated film and for a PNVP film annealed at 200 °C for 3 h. The assignment of the peaks from these spectra is summarized in Table 3. Direct comparison between the two spectra is not quantitative, since the thickness (and therefore the path length) of the two films was slightly different, due to the shrinking of the film upon annealing. It is obvious though that the width of the amide carbonyl peak (1755−1590 cm^{-1}) increased

Table 3. FTIR Data for Untreated and Annealed PNVP Films; Selected CH Peak Areas Were Normalized against the Amide Peak Area in Each Spectrum

		normalized peak areas	
mode	range (cm^{-1})	untreated PNVP	annealed PNVP
CH bending	1475−1410	0.185 ± 0.013	0.099 ± 0.009
CH bending	1305−1260	0.141 ± 0.007	0.061 ± 0.006
amide C═O stretching	1755−1590		

after the heat treatment. This is indicative of an overlapping of contributions from amide groups lying in at least two different environments. This probably means that the types of bonds involving the carbons close to the amide group in the pyrrolidone ring were partially modified. It may also indicate a partial oxidation of the amide group to form a carboxylic group that typically absorbs in the range 1780−1710 cm^{-1} in the solid state. The amide functionality (and hence intact pyrrolidone groups) remained abundant after annealing.

These spectra also indicate a change in the CH composition before and after annealing. The areas of the CH bending peaks in the ranges 1475−1410 cm^{-1} and 1305−1260 cm^{-1} were calculated. To have a measurement independent of the thickness of the film and to be able to compare data from the two different sets of samples, the areas of the peaks were normalized by the area of the amide carbonyl peak (1755−1590 cm^{-1}) within each spectrum. The values were then averaged over five different samples for each set. Assuming the amide carbonyl peak area to be constant, the normalized areas were different in the annealed film, with a 50% reduction in the CH peak areas after annealing.

Cross-Linking Process: Dependence on Annealing Time and Temperature. The degree of PNVP cross-linking was investigated by spectroscopic ellipsometry in the temperature range between 160 and 200 °C for periods of annealing time between 30 min and 3 h. This was done by measuring the percentage of the initial PNVP film that remained after thermal annealing at different annealing times and temperatures, and after rinsing the film in 150 mL of MILLI-Q water.

At the lower temperature (160 °C), no cross-linking occurred for up to 3 h annealing, as the PNVP films could be entirely washed away by 150 mL of MILLI-Q water (data not shown). Similarly, after annealing at 170 °C for 30 min, the PNVP films were still entirely water-soluble. The data presented in Figure 6 demonstrated that the films underwent a gradual compaction as a consequence of cross-linking which led to an initial slight decrease in film thickness (confirming X-ray and neutron reflectivity results). After this compaction, a film thickness decrease could be seen upon rinsing only if there was incomplete cross-linking, i.e. after annealing at the lower temperature (170 and 180 °C), or after annealing at 200 °C for times shorter than 1 h. After annealing for 1−3 h at 200 °C, the film was completely insoluble in water, so no thickness change was observed upon rinsing.

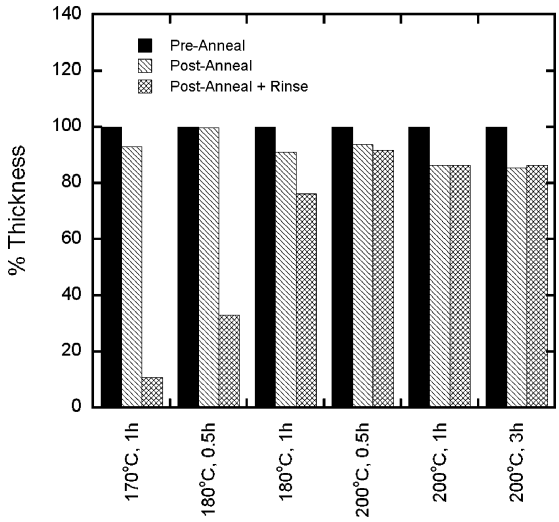

FIGURE 6. Percentage of PNVP film thickness change as a function of annealing time and temperature, and as a function of rinsing. The initial film thickness measured by spectroscopic ellipsometry is compared to the thickness after annealing at temperatures of 170, 180, and 200 °C, and then again after rinsing with 150 mL of MILLI-Q water. Each ellipsometric thickness measurement was taken two or three times. The error in the measurements is between 0.3 and 2.4%, except for the sample annealed at 170 °C for 1 h, where the error is 11.6%, and the sample annealed at 180 °C for 30 min, where the error is 10.4%.

Reflectivity data showed clearly that the film density and composition kept changing upon annealing at 200 °C between 30 min and 3 h (Figures 3 and 4). We believe that although the films become insoluble after just 60 min at 200 °C, complete cross-linking occurs after 3 h. The cross-linking was only partial for intermediate values of both annealing time and temperature. A trend was clearly visible from the data: increasing the annealing time and/or the annealing temperature increased the degree of cross-linking throughout the film.

Film Stability in Solvents. Annealed PNVP films were found to be highly resistant to a range of solvents, including water, ethanol and a solution of peroxide in concentrated sulphuric acid (see below). The change of solubility of the PNVP in water could be easily estimated by eye (see the Supporting Information, Figure S5), as the fully annealed films could not be dissolved by immersion in water. Figure S6 (see the Supporting Information) shows the thickness measured by ellipsometry of PNVP films annealed for 3 h at 200 °C, following immersion in water at 37 °C for different periods of time. These measurements indicate that the film thickness is unchanged after immersion in water for up to 3 weeks. The slight variability in the normalized thickness was most likely due to residual adsorbed water on the hydrophilic surface of the polymer after drying.

The measurement of the contact angle of a sessile droplet of water on clean silicon wafers (around 7°) and on annealed PNVP films (around 20°) was used to derive information on the solubility of annealed PNVP in different solvents. From these wettability measurements we could deduce that annealed PNVP films were not only stable in water at 37 °C for three weeks, but also in boiling water for up to 10 min, NoChromix solution (Sigma-Aldrich, inorganic peroxide-based oxidizing agent in concentrated sulphuric acid, similar to the well-known "piranha solution") for up to 10 min at room temperature, and after rinsing with ethanol. The only effective treatment found to completely remove the film from the wafer was exposure to an air plasma cleaner at a power of 29 W for more than 1 h.

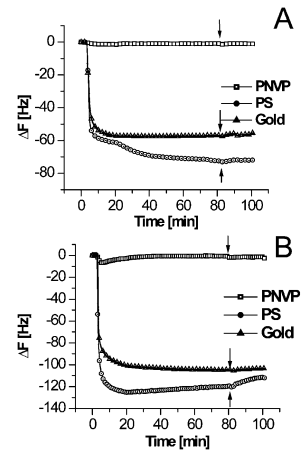

FIGURE 7. QCM analysis of (A) immunoglobulin G and (B) fibrinogen adsorption on PNVP films, PS films, and bare gold QCM crystal. The arrows indicate the flushing of the surface with fresh PBS to remove unbound protein.

Protein Adsorption on PNVP Coatings. Quartz crystal microbalance (QCM) measurements provide a very sensitive technique for the detection of adsorbed mass on a surface. Shifts in the resonant frequency of a QCM crystal are proportional to the change in its mass, with a negative shift indicating an increase in mass. Figure 7 shows QCM profiles obtained for the adsorption of fibrinogen (FGN) and IgG on completely cross-linked PNVP films, as well as on PS films and on bare gold surfaces (uncoated QCM crystal). FGN and IgG were chosen because of their different structure and net charge. FGN was also chosen because it is one of the proteins that trigger inflammatory response to foreign bodies in mammals (47). The protein solution concentrations were both 1 mg/mL (in PBS), a value close to that present in human plasma (48). The analysis was performed at 37 °C to mimic protein adsorption under physiological conditions.

As shown in Figure 7, FGN and IgG adsorbed strongly on the two control surfaces (PS and gold) as evidenced by the strong negative frequency shift measured upon injection of the protein solution. The frequency shift decreased rapidly in the first 10 min of exposure of the surfaces to the protein solution. With time the number of adsorption sites available decreased and the adsorbed mass reached a plateau value. When the surfaces were rinsed with PBS (indicated in Figure 7 by the arrows) a small positive frequency shift was observed, indicating that a small amount protein desorbed from the PS and gold surfaces. However, the bulk of the adsorbed protein remained on the surface, indicating a strong interaction between the proteins and the two substrates.

In the case of the annealed PNVP film, the frequency shift observed was minimal and barely detectable in comparison with the control surfaces. This indicated that almost no protein adsorbed onto the annealed PNVP surface. Using the Sauerbrey equation (Methods section) the frequency shift

Table 4. Frequency Shifts and Proteins Adsorbed Mass on Different QCM Sensors

	Δf (Hz)	Δm (ng/cm^2)
IgG on PS	−73.1	1312
IgG on gold	−57.2	1028
IgG on PVNP	−1.1	21
FGN on PS	−120.4	2162
FGN on gold	−105.0	1876
FGN on PNVP	−1.9	34

can be converted into the adsorbed protein mass. The results were slightly overestimated because the adsorbed protein layer was not rigid and included water. The results are summarized in Table 4: the adsorbed mass of IgG and FGN on the PNVP films was 21 and 34 ng/cm^2, respectively, values close to those obtained on well-known antifouling coatings such as PEG-based systems (cf. 10−30 ng/cm^2 in ref 49).

DISCUSSION

The above results illustrate the cross-linking behavior of PNVP thin films following thermal treatment. The thermal and phototreatment of PNVP have been investigated before, but a thermal cross-linking mechanism has never been investigated in detail before. It is known that the thermal treatment of PNVP in oxygen atmosphere gives rise to volatile degraded products at lower temperatures than in inert atmosphere (43), but most degraded products occur at temperatures above those considered in our study (200−400 °C). At these higher temperatures, the presence of an oxygen atmosphere gives rise to the formation of peroxide residues, which easily decompose, and give rise to the formation of active radicals (43). The mechanism of photooxidation of PNVP films under UV light leads primarily to the formation of insoluble fractions (42).

Our experimental observations seem to indicate that the main chemical reaction occurring upon thermal annealing is a cross-linking process. This process involves the CH groups on the pyrrolidone ring and on the backbone chain, without breaking the ring or involving the amide group (Figure 8). The thermal annealing allows the formation of radicals by homolytic cleavage of some of the C−H bonds. Radicals from different chains can then react to form interchain C−C bonds and thus create a network that is insoluble in water. A similar mechanism has been suggested previously for chemically activated processes (38). The coupling of radicals from different chains, which ultimately affects the cross-linking degree is here facilitated by the fact that the polymer is liquid at 200 °C, because its T_g is about 160 °C. The chains are more mobile in the molten moiety and the probability of two radicals to meet is higher than in the solid state.

Both the T_g and the liquid phase viscosity of a polymer increase with its molecular weight, so it could be postulated that the cross-linking process in the conditions used would be less efficient for much higher molecular weights. This would possibly lead to a network that retained some degree

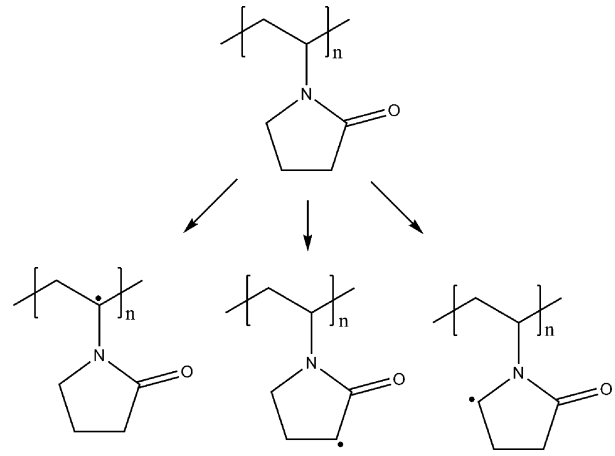

FIGURE 8. PNVP radical formation scheme proposed, similar to that for a chemically activated process (38). The radicals that can be formed are shown.

of solubility in water, making it a less desirable material to be used in a coating for biomedical applications because of leaching and deterioration issues.

Our FTIR data support such a reaction scheme, showing that the amount of C−H groups in the PNVP film decreased significantly after annealing. Moreover, the amide peak showed an increase in width after annealing, suggesting the presence of amide groups with different environments (different neighboring functional groups). Both results are in agreement with the cleavage of C−H bonds during the cross-linking process.

Reflectivity data also confirm the decrease in hydrogen content associated with the cleavage of C−H bonds during cross-linking. The combination of X-ray and neutron reflectometry measurements, in concert with the XPS data, can provide details of the composition and mass density of these annealed PNVP films. XPS measurements of the annealed film (3 h at 200 °C) suggested a C:N:O ratio of 73:11:16 (the hydrogen content for this film could not be determined using XPS). The neutron and X-ray scattering length density values for the PNVP film both depend on the mass density and the composition of the modified polymer. These two unknowns (mass density and H content) can thus be extracted from the refined X-ray and neutron reflectivity data (Table 2), leading to a mass density of 1.15 g/cm^3 (significantly denser than the as-prepared film) and a hydrogen content of 78 relative to the above C:N:O ratio. Thus, in comparison to the composition of the as-prepared film (C_6H_9NO, having a mass density of 0.79 g/cm^3), the film that was annealed for 3 h has an approximate composition of $C_6H_{6.4}N_{0.9}O_{1.3}$. As mentioned in the infrared spectroscopy results, the slight increase in the oxygen content is related to a mild degree of oxidation of the amide group.

The pyrrolidone ring, being neutral and hydrophilic, is mostly responsible for the low interaction between protein molecules and the polymer coating and appears not to be cleaved or altered during annealing to any significant degree, which explains the conservation of the low protein adsorbing properties of the polymer film after annealing. The QCM data clearly demonstrates the ability of the cross-linked PNVP

films to strongly repel different proteins compared to control surfaces such as gold and polystyrene. The calculated adsorbed mass can be compared to other types of antifouling coatings, such as those prepared by Zhang and co-workers (50). These authors prepared five thiol self-assembled monolayers on gold and three surface-initiated polymeric brushes, the latter with as little as 0.3 ng/cm^2 of FGN adsorbed. The PNVP films prepared in our study do not perform quite as well as the grafted polymer brushes prepared by Zhang and co-workers (50), but have the advantage that they do not require multistep processes often technically difficult to achieve and expensive to implement on a large scale or for large surface areas. Moreover, self-assembled monolayers on gold are unstable in the long term and are therefore likely only to be used in niche applications (51). The thermally annealed PNVP coatings prepared here are easily obtainable and have excellent repellent properties toward FGN and IgG, compared with similar PEG-based systems (49, 52, 53). An exciting result reported here is that PNVP coatings prepared here have better FGN repellent properties than grafted PNVP coatings obtained by surface initiated polymerization (16).

The influence of annealing time and annealing temperature on the cross-linking process was also investigated. The cross-linking process did not occur at 160 °C within the annealing times investigated, whereas cross-linking was observed throughout the film after annealing at 200 °C for as little as 30 min. The degree of cross-linking increased gradually with time, leading to densification of the film starting from the side closer to the heating source, and occurred rapidly at higher temperatures.

PNVP films prepared by the method proposed in this paper are stable for long periods of time in contact with water at the average human body temperature, making them suitable for the coating of implantable devices which can be heated or other materials and applications where low protein adsorption is required. For example, these PNVP coatings could easily be adapted to the fabrication of microfluidic devices for biotechnological application, as the microfluidic channels could be made protein repellent simply by flushing with PNVP solutions, drying, and annealing. The simplicity of the coating technique allows access to highly protein repellent surfaces in a cost-effective and convenient manner.

CONCLUSIONS

In this paper, for the first time, a thermally induced cross-linking mechanism for PNVP coatings was investigated, the treated films characterized, and their application as antifouling coatings ascertained. The cross-linking process most likely takes place via radical reactions at C—H bonds and does not require the breaking of the pyrrolidone ring. The cross-linking rate increased with the annealing temperature, occurring within a few hours at 200 °C. The excellent protein repellent properties of the PNVP were fully maintained after cross-linking, and make these coatings valid alternatives to grafted PEG coatings, widely used for their antifouling properties but more complicated to prepare. The cross-linked films were insoluble in water and other harsh solvents and stable in water for weeks, opening a wide range of applications for antifouling PNVP coatings. Simple and cost-effective techniques such as dip-coating could be implemented to prepare the films, potentially allowing the coating of objects of large surface area and complex geometries, demonstrating that the cross-linked PNVP coatings could be suitable for improving the biocompatibility of in vivo devices, such as catheters.

Acknowledgment. A.M.T. acknowledges the University of Sydney for funding and the support of CSIRO via the provision of a CSIRO Flagship Collaboration Fund Postgraduate Scholarship. C.N. acknowledges funding from the Australian Research Council.

Supporting Information Available: DSC, AFM, and neutron and X-ray reflectivity data, as well as optical micrographs and ellipsometry measurements of the effect of water on untreated and annealed PNVP films (PDF). This material is available free of charge via the Internet at http://pubs.acs.org.

REFERENCES AND NOTES

(1) Katti, K. S. *Colloids Surf., B* **2004**, *39* (3), 133–142.
(2) Wilson, B. S.; Lawson, D. T.; Muller, J. M.; Tyler, R. S.; Kiefer, J. *Annu. Rev. Biomed. Eng.* **2003**, *5*, 207–249.
(3) Thierry, B.; Tabrizian, M. *J. Endovascular Ther.* **2003**, *10* (4), 807–824.
(4) Wilson, G. S.; Gifford, R. *Biosens. Bioelectron.* **2005**, *20* (12), 2388–2403.
(5) Wisniewski, N.; Moussy, F.; Reichert, W. M. *Fresenius' J. Anal. Chem.* **2000**, *366* (6), 611–621.
(6) Wang, J. *Electroanalysis* **2001**, *13* (12), 983–988.
(7) Andrade, J. D.; Hlady, V. *Adv. Polym. Sci.* **1986**, *79*, 1–63.
(8) Ratner, B. D.; Hoffman, A. S.; Schoen, F. J.; Lemons, J. E., *Biomaterials Science: An Introduction to Materials in Medicine*, first ed.; Academic Press: New York, 1997.
(9) Fang, C.; Zhang, M. *J. Mater. Chem.* **2009**, *19* (35), 6258–6266.
(10) Anderson, J. M.; Shive, M. S. *Adv. Drug Delivery Rev.* **1997**, *28* (1), 5–24.
(11) Anderson, J. M.; Rodriguez, A.; Chang, D. T. *Semin. Immunol.* **2008**, *20* (2), 86–100.
(12) McArthur, S. L.; McLean, K. M.; St. John, H. A. W.; Griesser, H. J. *Biomaterials* **2001**, *22*, 3295–3304.
(13) Harris, J. M.; Zalipsky, S., *Poly(ethylene glycol): Chemistry and Biological Applications*; American Chemical Society: Washington, D.C., 1997; p 489.
(14) Szleifer, I. *Curr. Opin. Solid State Mater. Sci.* **1997**, *2*, 337–344.
(15) Kingshott, P.; Griesser, H. J. *Curr. Opin. Solid State Mater. Sci.* **1999**, *4*, 403–412.
(16) Wu, Z.; Chen, H.; Liu, X.; Zhang, Y.; Li, D.; Huang, H. *Langmuir* **2009**, *25* (5), 2900–2906.
(17) Feng, W.; Zhu, S. P.; Ishihara, K.; Brash, J. L. *Biointerphases* **2006**, *1* (1), 50–60.
(18) Ma, Z. W.; Mao, Z. W.; Gao, C. Y. *Colloids Surf., B* **2007**, *60*, 137–157.
(19) Ostuni, E.; Chapman, R. G.; Holmlin, R. E.; Takayama, S.; Whitesides, G. M. *Langmuir* **2001**, *17* (18), 5605–5620.
(20) Werner, C.; Maitz, M. F.; Sperling, C. *J. Mater. Chem.* **2007**, *17* (32), 3376–3384.
(21) Higuchi, A.; Shirano, K.; Harashima, M.; Yoon, B. O.; Hara, M.; Hattori, M.; Imamura, K. *Biomaterials* **2002**, *23* (13), 2659–2666.
(22) Marchant, R. E.; Johnson, S. D.; Schneider, B. H.; Agger, M. P.; Anderson, J. M. *J. Biomed. Mater. Res.* **1990**, *24* (11), 1521–1537.
(23) Wetzels, G. M. R.; Koole, L. H. *Biomaterials* **1999**, *20* (20), 1879–1887.
(24) Robinson, S.; Williams, P. A. *Langmuir* **2002**, *18* (23), 8743–8748.
(25) Robinson, B. V.; Sullivan, F. M.; Borzelleca, J. F.; Schwartz, S. L. *PVP, A Critical Review of the Kinetics and Toxicology of Polyvinylpyrrolidone (Povidone)*; Lewis Publisher: Boca Raton, FL, 1990.

(26) Smith, L. E.; Rimmer, S.; MacNeil, S. *Biomaterials* **2006**, *27* (14), 2806–2812.
(27) Davies, W. L.; Gloor, W. T. *J. Pharm. Sci.* **1972**, *61* (4), 618–&.
(28) Hoang, T.; Jorgensen, M. G.; Keim, R. G.; Pattison, A. M.; Slots, J. *J. Periodontal Res.* **2003**, *38* (3), 311–317.
(29) Reimer, K.; Vogt, P. M.; Broegmann, B.; Hauser, J.; Rossbach, O.; Kramer, A.; Rudolph, P.; Bosse, B.; Schreier, H.; Fleischer, W. *Dermatology* **2000**, *201* (3), 235–241.
(30) Vogel, F. G. M. *Soap Cosmet. Chem. Specialties* **1989**, *65* (4).
(31) Yañez, F.; Concheiro, A.; Alvarez-Lorenzo, C. *Eur. J. Pharm. Biopharm.* **2008**, *69* (3), 1094–1103.
(32) Ravin, H. A.; Seligman, A. M.; Fine, J. *New Engl. J. Med.* **1952**, *247* (24), 921–929.
(33) Hamidi, M.; Azadi, A.; Rafiei, P. *Adv. Drug Delivery Rev.* **2008**, *60* (15), 1638–1649.
(34) Liu, Z.; Rimmer, S. *J. Controlled Release* **2002**, *81* (1−2), 91–99.
(35) Jeon, S. I.; Lee, J. H.; Andrade, J. D.; de Gennes, P. G. *J. Colloid Interface Sci.* **1991**, *142* (1), 149–158.
(36) Sharma, S.; Johnson, R. W.; Desai, T. A. *Biosens. Bioelectron.* **2004**, *20*, 227–239.
(37) Meinhold, D.; Schweiss, R.; Zschoche, S.; Janke, A.; Baier, A.; Simon, F.; Dorschner, H.; Werner, C. *Langmuir* **2004**, *20* (2), 396–401.
(38) Barros, J. A. G.; Fechine, G. J. M.; Alcantara, M. R.; Catalani, L. H. *Polymer* **2006**, *47* (26), 8414–8419.
(39) Kuypers, M. H. Method of providing a substrate with a layer comprising a poly vinyl base hydrogel and a biochemically active material. European Patent 0363504, 1990.
(40) Rosiak, J. M.; Olejniczak, J. *Radiat. Phys. Chem.* **1993**, *42*, 903–906.
(41) Rosiak, J. M.; Ulanski, I. P.; Pajewski, L. A.; Yoshii, F.; Makuuchi, K. *Radiat. Phys. Chem.* **1995**, *46*, 161–168.
(42) Hassouna, F.; Therias, S.; Mailhot, G.; Gardette, J.-L. *Polym. Degrad. Stab.* **2009**, *94* (12), 2257–2266.
(43) Peniche, C.; Zaldivar, D.; Pazos, M.; Paz, S.; Bulay, A.; Roman, J. S. *J. Appl. Polym. Sci.* **1993**, *50*, 485–493.
(44) James, M.; Nelson, A.; Brule, A.; Schulz, J. C. *J. Neutron Res.* **2006**, *14* (2), 91–108.
(45) Nelson, A. *J. Appl. Crystallogr.* **2006**, *39*, 273–276.
(46) Peniche, C.; Zaldivar, D.; Pazos, M.; Paz, S.; Bulay, A.; San Roman, J. *J. Appl. Polym. Sci.* **1993**, *50*, 485–493.
(47) Tang, L.; Eaton, J. W. *J. Exp. Med.* **1993**, *178* (6), 2147–2156.
(48) Lowe, G. D. O.; Rumley, A.; Mackie, I. J. *Ann. Clin. Biochem.* **2004**, *41*, 430–440.
(49) Jo, S.; Park, K. *Biomaterials* **2000**, *21* (6), 605–616.
(50) Zhang, Z.; Zhang, M.; Chen, S.; Horbett, T. A.; Ratner, B. D.; Jiang, S. *Biomaterials* **2008**, *29* (32), 4285–4291.
(51) Schlenoff, J. B.; Li, M.; Ly, H. *J. Am. Chem. Soc.* **1995**, *117* (50), 12528–12536.
(52) Volden, S.; Zhu, K.; Nyström, B.; Glomm, W. R. *Colloids Surf., B* **2009**, *72* (2), 266–271.
(53) Rastogi, A.; Nad, S.; Tanaka, M.; Mota, N. D.; Tague, M.; Baird, B. A.; Abrunlfa, H. c. D.; Ober, C. K. *Biomacromolecules* **2009**, *10* (10), 2750–2758.

AM100406J